IIETA International Information and Engineering Technology Association
Advancing the World of Information and Engineering

Traitement du Signal
Vol. 39, No. 1, February, 2022, pp. 355-362
Journal homepage: http://iieta.org/journals/ts

Acupoint Selection for Autonomous Massage Based on Infrared Thermography

Jianfeng Shu[1], Rongtao Ding[2], Aixiang Jin[3], Hui Zhu[3], Shu Chen[4*]

[1] Department of Acupuncture and Massage, Zhejiang Provincial People's Hospital, People's Hospital of Hangzhou Medical College, Hangzhou 310014, China
[2] School of E-commerce, Zhejiang Business College, Hangzhou 310053, China
[3] Department of Head, Neck & Thyroid Surgery, Zhejiang Provincial People's Hospital, People's Hospital of Hangzhou Medical College, Hangzhou 310014, China
[4] Department of Rehabilitation Medicine, Zhejiang Provincial People's Hospital, People's Hospital of Hangzhou Medical College, Hangzhou 310014, China

Corresponding Author Email: shushu626@126.com

https://doi.org/10.18280/ts.390137

Received: 10 October 2021
Accepted: 28 December 2021

Keywords:
infrared thermography, temperature specificity, image preprocessing, edge detection, acupoint positioning

ABSTRACT

After breast cancer surgery, the patient has difficulty in selecting the acupoints for autonomous massage, due to the changes in muscles and nerves on the affected side. To overcome the difficulty, this paper proposes an acupoint selection method for autonomous massage after breast cancer surgery, based on infrared thermography. Firstly, the contrast of the infrared thermogram was enhanced by image differencing, and the chest region and upper limbs were segmented through global thresholding. Next, temperature specific detection and edge detection algorithms were combined to automatically locate the main chest organs, and the horizontal and vertical axes of the upper limbs, according to the temperature specificity and temperature variation induced by the physiological structure of chest and upper limbs. Furthermore, the main acupoints for autonomous massage were determined, based on their positions relative to the axes of main organs. Experimental results show that our method achieved a positioning accuracy greater than 90.12%. The excellent positioning effect improves the compliance of patients in active rehabilitation.

1. INTRODUCTION

After modified radical mastectomy, breast cancer patients will face pain on the affected side, formation of scar tissues, and shoulder movement disorder, owing to the loss of some muscles and the damages of nerves and blood vessels. These complications will lower the survival quality of the patients. Tachibana et al., Takayama et al., and Klassen et al. [1-3] demonstrated that acupoint massage can promote the backflow of lymph fluid by stimulating the specific acupoints of the body, which in turn boosts the absorption of inflammatory substances, expands blood vessels, and increases the strength of limb muscles. Liu and Wan [4, 5] proved that acupoint massage can dredge the channels, promote qi to activate blood, and relieve swelling and pain; these functions help to alleviate the upper limb edema after the surgery, and assist the patient to recover from upper limb dysfunction. Fink et al. and Ijaz et al. [6, 7] suggested that acupoint massage, coupled with continuing nursing, has a positive effect on the quality of life and immune function of breast cancer patients after the surgery, and improves their sleep quality and negative emotions. However, the acupoint massage in rehabilitation after breast cancer surgeries is entirely dependent on doctors, causing a strain of medical resources. Besides, the patient has difficulty in selecting the acupoints for autonomous massage, due to the changes in muscles and nerves on the affected side, and his/her limited cognitive ability. Therefore, the development of effective and feasible automatic acupoint positioning techniques becomes a new focal point in the research of clinical medical care. By virtue of the special functions of digital imaging, automatic acupoint positioning aims to pinpoint the acupoints that are difficult to locate, and promote the scientific, humanity, and intelligent level of acupuncture and massage.

Elahee et al. and Chang et al. [8, 9] testified that, during the modernization of traditional Chinese medicine (TCM), infrared thermography plays an important role in the dialectical diagnosis of the TCM, and the exploration of channels and acupoints. Huang et al. and Shen et al. [10, 11] proposed that the infrared radiation of human acupoints contains important physiological, and pathological information, and clinically observed specific changes in infrared radiation of the channels and acupoints in various diseases. Beast cancer surgeries cause inflammatory response and abnormal blood operation, resulting in an abnormal surface temperature distribution in the lesion area on the affected side. Starting from the temperature specificity of different organs or lesions, infrared thermography can detect the significant differences in the reflectance spectra of organ/acupoint areas and surrounding tissues. The differences reflect the disparity between organ/acupoint areas and non-organ/acupoint areas in physiological parameters.

This paper aims to overcome the low accuracy and difficulty of acupoint positioning by breast cancer patients after surgery. Therefore, an acupoint selection method was proposed for autonomous massage after breast cancer surgery, based on infrared thermography. Multiple channels were selected to observe the infrared radiation trajectories of the patient,

including the kidney channel of foot-Shaoyin, stomach channel of foot-Yangming, spleen channel of foot-Taiyin, liver channel of foot-Jueyin, pericardium channel of hand-Jueyin, and lung channel of hand-Taiyin. On this basis, temperature specific detection was combined with edge detection into an automatic acupoint positioning algorithm for infrared thermograms. There are two steps in our algorithm: local positioning, and global refinement. The algorithm makes full use of the correlation and mutation of human temperature, and identifies the main acupoints based on the prior knowledge of acupoint distribution in the TCM. The flow of our algorithm is shown in Figure 1.

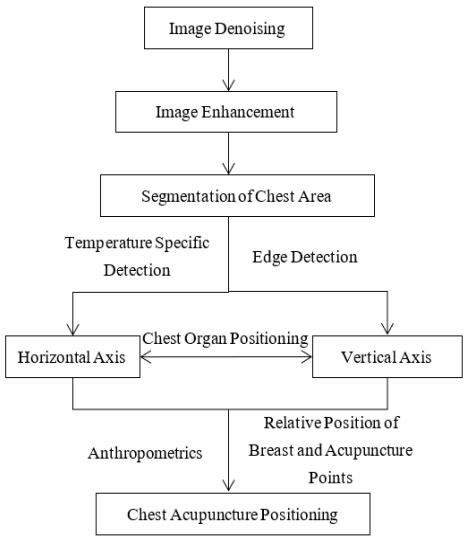

Figure 1. Flow of our automatic acupoint positioning algorithm

2. IMAGE PREPROCESSING

Image preprocessing is indispensable in medical image-assisted diagnosis, for preprocessing can eliminate irrelevant information from the image, and restore the useful true information [12]. The preprocessed data are relevant, detectable, and super concise, and contribute to the reliability of subsequent feature extraction, image segmentation, image matching, and target recognition. Here, every infrared thermogram is preprocessed in three steps: image denoising, image enhancement, and segmentation of chest and upper limb areas.

2.1 Image denoising

Medical infrared imagers mainly involve the photon noise generated by the background and signal itself. Studies have shown that the median filter is a simple and fast tool to filter out noises (especially pulse noise), while preserving the details (e.g., edges, and acute angles) of the signal. It is widely regarded as an excellent noise filter. In the field of medical image processing, the image processing ought to retain the useful original data, and only remove the noisy data. Therefore, this paper improves the median filter to eliminate image noises, while preserving image details as much as possible.

2.1.1 Standard median filter

The median filter implements a neighborhood operation similar to convolution. Rather than weighted summation, the operation ranks the pixels in the neighborhood by grayscale, and selects the median as the output pixel value. For an N*N median filter, if the grayscale of the input pixel is greater than or equal to that of $(N^2\text{-}1)/2$ pixels in the neighborhood, and smaller than or equal to $(N^2\text{-}1)/2$ pixels in the neighborhood, then the grayscale of that pixel will be taken as the output grayscale.

Definition: Let $f_{m,n}(x, y)$ be an $m \times n$ digital image; A be the filter window of the size $N = (2k + 1) \times (2k + 1)$. Then, the two-dimensional (2D) median filter of image $f_{m,n}(x, y)$ can be expressed as:

$$f'_{m,n}(x,y) = med_N \{ f_{m,n}(x,y) \} \tag{1}$$

During image processing, the 2D median filter firstly expands the start and end of the rows and columns of image data by k points, and then sets a filter window to transverse all the points on the original image. The central point value of the window is replaced with the median of the original values in the window.

2.1.2 Improved median filter

The improved median filter can be described as follows:

Step 1. Find the difference between the original image and the image processed by the median filter:

$$d_{m,n}(x,y) = f_{m,n}(x,y) - med_N \{ f_{m,n}(x,y) \} \tag{2}$$

Step 2. Smoothen the original image, and convolute it with an $(k \times k)$ 2D Gaussian kernel $g_{k,\sigma}(x, y)$:

$$s_{m,n}(x,y) = f_{m,n}(x,y) \times g_{k,\sigma}(x,y) \quad \{k < m, n\} \tag{3}$$

The Gaussian convolution can be described as a 2D Gaussian distribution with zero mean:

$$g(x,y) = \frac{1}{\sigma\sqrt{2\pi}} e^{-\frac{1}{2}\left(\frac{x+y}{\sigma}\right)^2} \tag{4}$$

The Gaussian kernel must be censored in a proper range, as the Gaussian distribution falls between $-\infty$ and ∞. The Gaussian kernel in the algorithm is a square, where each side is as wide as $[2 \times 2(\sigma + 1) + 1]$ pixels. This means the Gaussian kernel needs to be censored at $\pm 2(\sigma + 1)$. The σ value determines the smoothness of Gaussian convolution, which in turn decides how much image details are preserved.

(3) Find the absolute difference between the original image and the smoothened image:

$$v_{m,n}(x,y) = \left| f_{m,n}(x,y) - s_{m,n}(x,y) \right| \tag{5}$$

The difference reflects the degree of change of the image. The Gaussian convolution of $v_{m,n}(x, y)$ yields a smooth form:

$$sv_{m,n}(x,y) = v_{m,n}(x,y) \times g_{k,\sigma}(x,y) \quad \{k < m, n\} \tag{6}$$

Step 4. Find the ratio between the difference (2) and the change induced by smoothing:

$$r_{m,n}(x,y) = \frac{d_{m,n}(x,y)}{sv_{m,n}(x,y)} \tag{7}$$

The difference between the original image and the median filtered image is then divided by the image smoothened by Gaussian convolution. The ratio of each pixel is compared with the threshold. If the ratio is greater than the threshold, then the corresponding pixel will be replaced with the filtered pixel value; otherwise, preserve the pixel value of the original image. The threshold is calculated automatically. Thus, 7-9% of the pixels in the original image will be replaced.

As shown in formula (7), during the division operation, the denominator is the image obtained by Gaussian convolution. Some pixels in the image may be zero. These pixels must be excluded to prevent the denominator from being zero. The numerator $d_{m,n}(x, y)$ may be relatively large in the presence of noises or fine details. However, the denominator $sv_{m,n}(x, y)$ becomes smaller in the presence of noises, and larger in the presence of fine details (high change rate). This provides negative feedback to allow the filter see fine details.

There are two parameters in the adaptive median filter: the size N of window template, and σof Gaussian convolution. The size N determines the range of median. It is selected similarly as that of the standard median filter. Here, the 3*3 template is selected. The value of σ determines the smoothness of Gaussian convolution, and how much the image details is preserved. Through repeated tests, it was determined that σ=5.

2.2 Image enhancement

As the first step of preprocessing, image enhancement aims to enhance the contrast between pathological tissues and normal glandular tissues, and enlarge the suspicious image areas, highlighting valuable diagnostic information. This paper relies on image differencing to enhance images. Image differencing intends to extract the high-frequency information from the image. The temperature of acupoints / lesion areas is different from that of normal tissues. Therefore, the acupoints / lesion areas are brighter or darker than the surrounding normal tissues in the infrared thermogram. In the frequency domain, the acupoints / lesion areas exist as high-frequency signals submerged in ultra-high frequency noises and the low-frequency background. During image differencing, the image is firstly subjected to Laplace sharpening to enhance its high-frequency information. Then, the original image is subjected to median filter, which is comparable to smoothing, to obtain the low-frequency information. After that, the absolute value of the difference of the two resulting images is used to form another image, which is the target information. The image differencing algorithm is as follows:

The preprocessed image $f(x, y)$ is enhanced by Laplace operator. The Laplace transform of binary function $f(x, y)$ can be defined as:

$$\nabla^2 f = \frac{\partial^2 f}{\partial x^2} + \frac{\partial^2 f}{\partial y^2} \tag{8}$$

For discrete digital images, the Laplace operator can be defined as:

$$\nabla^2 f = \frac{\partial^2 f}{\partial x^2} + \frac{\partial^2 f}{\partial y^2} = f(x-1, y) + f(x+1, y) + f(x, y+1) + f(x, y-1) - 4f(x, y) \tag{9}$$

The sharpening is carried out by the following template:

$$\begin{pmatrix} -1 & -1 & -1 \\ -1 & 9 & -1 \\ -1 & -1 & -1 \end{pmatrix}$$

where, the black dot in the middle is the central element, i.e., the object to be processed. The image after Laplace sharpening is denoted as $f_{enhance}(x, y)$.

Next, image $f(x, y)$ is smoothened by the 3*3 template of the median filter to remove the high-frequency information, while preserving the low-frequency information (e.g., the background). The resulting image is denoted as $f_{smooth}(x, y)$. Then, the difference $f_{sub}(x, y)$ between images $f_{enhance}(x, y)$ and $f_{smooth}(x, y)$ can be expressed as:

$$f_{sub}(x, y) = f_{enhance}(x, y) - f_{smooth}(x, y) \tag{10}$$

During image differencing, the resulting image $f_{sub}(x, y)$ contains some negative values. In this paper, the negative values are set to zero or replaced with the absolute values, and the two cases are compared through experiments. Since the pixels with negative values belong to the low-frequency background, these pixels in the image obtained by differencing are set to zero:

$$f_{sub-true}(x, y) = \max(0, f_{sub}(x, y)) \tag{11}$$

Figure 2 shows the effect of denoising and enhancement of an infrared thermogram.

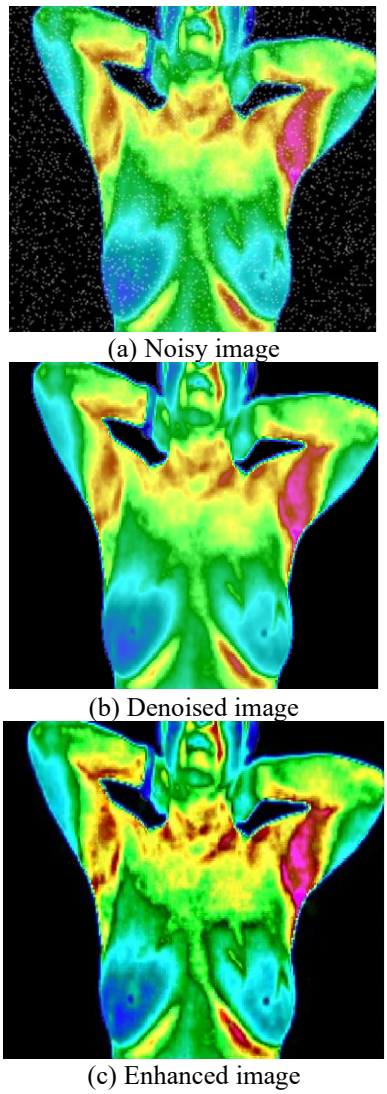

(a) Noisy image

(b) Denoised image

(c) Enhanced image

Figure 2. Effect of denoising and enhancement of an infrared thermogram

2.3 Segmentation of breast and upper limb areas

Most medical images are composed of a background and several targets. Doctors or computer automatic detection programs normally judge or process the main targets. Therefore, the task after greyscale normalization is to extract the targets from the chest infrared thermogram, i.e., remove the background, by a certain method. The most common way to complete the task is thresholding. This paper segments the original image through global thresholding, and optimizes the threshold iteratively. The specific steps are as follows:

Step 1. Solve the maximum grayscale R_{max} and minimum grayscale R_{min} of the image, and define the initial threshold as $T_0 = (R_{\max} + R_{\min})/2$.

Step 2. Segment the image into targets and background with threshold T_K, and solve the mean grayscale R_0 of targets and that R_B of background.

Step 3. Solve the new threshold T_{K+1}: $T_{K+1} = (R_0 + R_B)/2$.

Step 4. If $T_K = T_{K+1}$, terminate the algorithm; otherwise, K ←K+1, and jump to Step 2.

Figure 3(c) is the binary image obtained through thresholding.

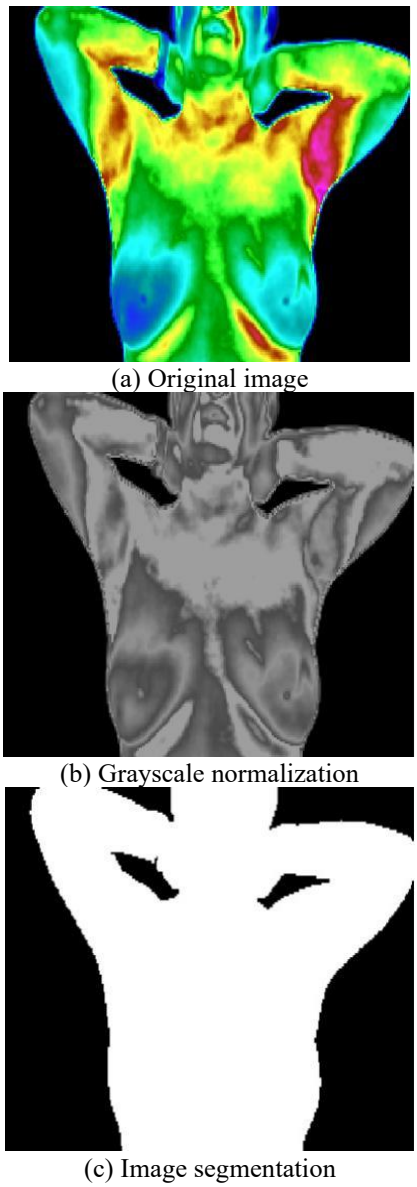

(a) Original image

(b) Grayscale normalization

(c) Image segmentation

Figure 3. Segmentation of chest and upper limb areas

3. POSITIONING OF CHEST ORGANS AND UPPER LIMBS

3.1 Temperature specificity-based positioning

On a healthy human body, the surface temperature tracks the distribution of qi, blood, yin, and yang. The governor channels are smooth, and the temperature is uniformly distributed horizontally. Therefore, most local temperatures in the chest infrared thermogram are strongly correlated, and slowly changing.

In some chest organs, however, the local temperature variation is intensified by the changes to the physiological structure and vessel distribution in local tissues [13]. The chest infrared thermogram features relatively high temperatures at concave parts of the body, such as supraclavicular fossae, armpits, navel, and groin, and relatively low temperatures at convex parts of the skin, namely, nipples, and breasts.

Therefore, the skin temperature distribution of the chest is specific, and related to the positions and physiological structure of chest organs. Thus, the chest organs can be positioned by the temperature specificity.

The above analysis shows that the local temperature specificity in the infrared thermogram can be expressed as the autocorrelation feature of temperature distribution in the area. The autocorrelation feature of a chest organ depends on its physiological structure. Let M be the matrix of the breast thermogram. Then, the autocorrelation function can be expressed as:

$$R_{x,y} = \sum_{u,v} (M(x+u, y+v) - M(x,y))^2 \tag{12}$$

where, $M(x, y)$ is the temperature at coordinates (x, y); $R_{x,y}$ is the mean temperature variation of the thermogram induced by a shift (u, v) of pixel (x, y), $(u, v)$is a hyperparameter that can be configured during system experiments. Thus, matrix R describes the degree of changes in local temperature. The spatial information of a part with special temperature can be obtained by analyzing the extremums in R. This paper adopts the Harris algorithm [14] to detect temperature specificity. The basic principle of the algorithm is to compute the temperature change after a small window, centering at the target pixel, moves along any direction, and express the temperature change analytically. Let u and v be the moving distances of the small window centering at pixel (x, y) along the x and y directions, respectively. The analytical expression of the temperature change can be given by the Harris algorithm as:

$$\begin{aligned} R_{x,y} &= \sum w_{x,y} (M_{x|u,y|v} - M_{x,y}) \\ &= \sum w_{x,y} (u\frac{\partial M}{\partial X} + V\frac{\partial M}{\partial Y} + o(\sqrt{u^2+v^2}))^2 \end{aligned} \tag{13}$$

where, $R_{x,y}$ is the temperature change in the window; $w_{x,y}$ is the window function, which is generally defined as $w_{x,y} = e^{(x^2+y^2)/\sigma^2}$; M is the function of the infrared thermogram. Without considering the infinitesimal terms:

$$\begin{aligned} R_{x,y} &= \sum w_{x,y} [u^2 (M_x)^2 + v^2 (M_y)^2 + 2uvM_x M_y] \\ &= Au^2 + 2Cuv + Bv^2 \end{aligned} \tag{14}$$

The quadratic form of $R_{x,y}$ can be expressed as:

$$R_{x,y} = \begin{bmatrix} u\,v \end{bmatrix} E \begin{bmatrix} u \\ v \end{bmatrix} \tag{15}$$

E is a real symmetric matrix:

$$E = \sum w_{x,y} \begin{bmatrix} I_x^2 & I_x \bullet I_y \\ I_x \bullet I_y & I_y^2 \end{bmatrix} \tag{16}$$

Through diagonalization:

$$R_{x,y} = T^{-1} \begin{pmatrix} \lambda_1 & 0 \\ 0 & \lambda_2 \end{pmatrix} T \tag{17}$$

where, T is the rotation factor. The diagonalization does not change the shape of the spatial curved surface with u and v as the coordinates. The eigenvalues represent the curvature of the image surface in the directions of the two principal axes. When the two eigenvalues are relatively small, the vicinity of the target pixel is a flat area; When one eigenvalue is large and the other is small, the feature point is on the edge; Only when both eigenvalues are relatively large, the temperature will change violently, due to the movement in any direction. Thus, the Harris corner response function can be obtained:

$$CRF(x, y) = \det(E) - k(tr(E))^2 \tag{18}$$

where, det(E) is the determinant of matrix E; tr(E) is the trace of the matrix. The target pixel is a corner, when its CRF value is greater than a given threshold.

According to its physical meaning, the CRF of the matrix is the temperature specific distribution of image M. In the matrix, the value of a pixel is negatively correlated with the temperature autocorrelation at the point, and positively correlated with the temperature specificity at the point. In this way, it is possible to obtain a chest temperature specific distribution image, which only contains organ distribution features (Figure 4).

As shown in Figure 4, after the removal of edge information of the chest, the main specific areas include supraclavicular fossae, armpits, anterior median line, nipples, and breasts. These areas are effective objects with strong temperature specificity, and always appear in the temperature specific distribution images of every subjects.

Figure 4. Temperature specific distribution after removal of disturbance

3.2 Edge feature-based positioning

In the infrared thermogram, the organs with drastic changes in temperature autocorrelation can be located by detecting temperature specificity. However, temperature specific detection cannot effectively locate the upper limb areas, for their insignificant changes of temperature autocorrelation. Considering the obvious edge features of arms and shoulders, the edge detection was adopted to position these areas. To ensure positioning accuracy and control the computing load, the edges were detected by Log operator from chest infrared thermogram [15]. Normally, the image is filtered by Gaussian function, and the second-order derivative is solved for the filtered image:

$$\nabla^2[G(x, y) * f(x, y)] = \nabla^2 G(x, y) * f(x, y) \tag{19}$$

where, $\nabla^2 G(x, y)$ is the Log operator:

$$\nabla^2 G(x, y) = \frac{1}{2\pi\sigma^4}\left[\frac{x^2 + y^2}{\sigma^2} - 2\right] e^{-\frac{x^2+y^2}{2\sigma^2}} \tag{20}$$

After $\nabla^2 G(x, y)$ operation on image $f(x, y)$, the edge points, i.e., the zero crossing points are searched for. Figure 5 presents the edges extracted from Figure 3.

Figure 5. Results of edge extraction

4. ACUPOINT POSITIONING

This paper locates chest acupoints with the chest organ positions as the coordinates. In TCM theories, acupoint positioning is based on the organ distribution of the subject, using the organ distance ratio as the standard unit [16]. From the angle of anthropometry [17], acupoint positioning in TCM theories is a relative positioning method, which ensures that the same positioning standard applies to different objects. After breast cancer surgery, the acupoint positions may be shifted or affected by the growth of scars and local inflammatory substances. After consulting professional acupuncturists, the affected acupoints are summarized as Table 1. Referring to the national standard wall chart of channels and acupoints [18], the exact positions of the acupoints on the front of the chest and upper limbs can be obtained as Figure 6.

To position more chest features, this paper locates chest organs in the light of both temperature specificity and edge

features. The two types of features were integrated to pinpoint supraclavicular fossae, armpits, anterior median line, nipples, and breasts. In anthropometric research, every textbook and national standard of acupuncture specify acupoint positions, which are determined based on the measured data on the organs of numerous people in different races. The main acupoint on the chest can be determined, according to the known positions of anterior median line, nipples, armpits, and supraclavicular fossae, and positioned in the coordinate system by the relative position between acupoints. The position of each organ can be marked by a blue line (zero temperature) in the coordinate system. The coordinate system of chest features is illustrated in Figure 7. From top to bottom, the horizontal lines represent the horizontal centers of supraclavicular fossae, the centers of armpits, the horizontal position of the left nipple, and the horizontal position of the right nipple, respectively; From left to right, the vertical lines represent the midline of the left armpit, the midline of the left nipple, the midline of the left clavicle, anterior median line, the midline of the right armpit, the midline of the right nipple, and the midline of the right clavicle, respectively. Based on the coordinates of these organs, it is possible to locate the main acupoints in the chest area, and divide the regions of interest (ROIs).

Table 1. The acupoints affected by breast cancer surgery

Serial number	Trajectory along channel	Affected acupoint
1	Kidney channel of foot-Shaoyin	Bulang, Shenfeng, Lingxu
2	Stomach channel of foot-Yangming	Wuyi, Yingchuang, Ruzhong, Rugen
3	Spleen channel of foot-Taiyin	Shidou, Tianxi, Xiongxiang
4	Liver channel of foot-Jueyin	Qimen
5	Pericardium channel of hand-Jueyin	Tianchi
6	Lung channel of hand-Taiyin	Zhongfu

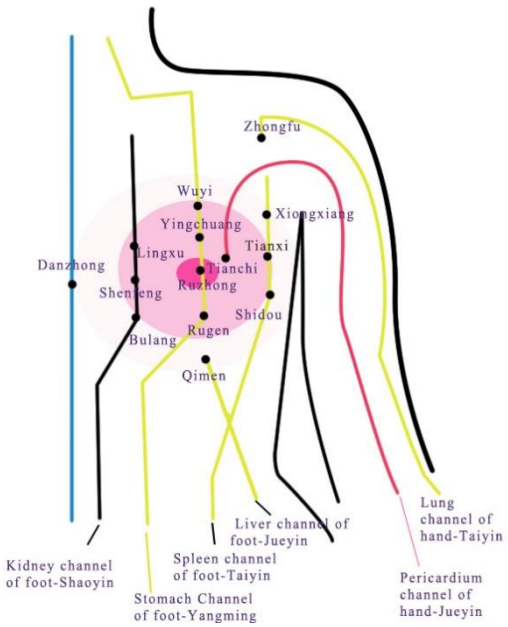

Figure 6. Positions of the acupoints on the front of the chest and upper limbs

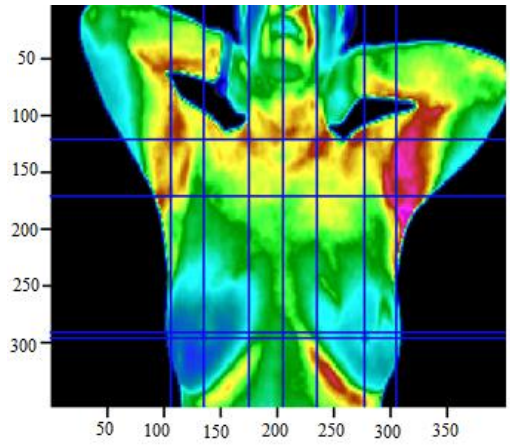

Figure 7. Coordinate system of chest features

In TCM, the chest acupoints are selected with anterior median line as the marker line of the front chest, i.e., the vertical midline in the front of breastbones. Danzhong acupoint lies on the anterior median line, and exists as the midpoint of the line connecting the two nipples. Thus, the horizontal coordinate of Danzhong acupoint can be derived from the horizontal coordinates of the two nipples, and its precise position can be obtained in view of the vertical coordinate of the anterior median line.

Acupoints Bulang, Shenfeng, and Lingxu fall on the same vertical line, and between the midsternal line and the midclavicular line. All of them are located at 2 inches (about 6.67cm, i.e., the total width of three fingers) next to the anterior median line.

Shenfeng acupoint has the same horizontal coordinate as Danzhong acupoint. Bulang acupoint is one rib below Shenfeng acupoint. Lingxu acupoint is one rib above Shenfeng acupoint. According to anthropometry, the normal thickness between ribs is 3.8cm for females. Then, the positions of acupoints Bulang, Shenfeng, and Lingxu can be determined.

The other acupoints can be pinpointed similarly. Acupoints Wuyi, Yingchuang, Ruzhong, and Rugen all fall on the midlines of nipples. Among them, Wuyi lies in the second intercostal space, 4 inches from the anterior median line. It is 2 intercostal spaces above the nipples along the midlines of nipples (the vertical lines passing the nipples). Yingchuang lies in the third intercostal space, 4 inches from the anterior median line. Ruzhong lies in the fourth intercostal space, at the center of each nipple, and 4 inches from the anterior median line. Rugen lies right below each nipple at the root of the corresponding beast, falling in the fifth intercostal space, 4 inches from the anterior median line.

The vertical coordinates of acupoints Shidou, Tianxi, and Xiongxiang are all 6 inches from the anterior median line. As shown in Figure 6, Tianxi and Tianchi belong to the same horizontal line. Therefore, it is necessary to locate Tianchi first. Horizontally, Tianchi lies 1 inch outside the corresponding nipple; Vertically, the acupoint is 5 inches from the anterior median line. Falling in the fourth intercostal space, Tianxi has the same horizontal coordinate as Tianchi, but its vertical coordinate is 6 inches from the anterior median line. Shidou lies in the fifth intercostal space, i.e., one rib below Tianxi. Xiongxiang lies in the third intercostal space, one rib above Tianxi.

Acupoint Qimen faces right toward the corresponding nipple, and lies 4 inches from the anterior median line. It is two ribs directly below Ruzhong (in the sixth intercostal

space). As for acupoint Zhongfu, the horizontal coordinate falls in the first intercostal space on the outside of the infraclavicular fossae, and 6 inches from the anterior median line. It is two ribs above Xiongxiang.

In this way, all acupoints in Table 1 can be positioned in turn. Figure 8 shows the acupoint positioning results of the infrared thermogram of the front chest.

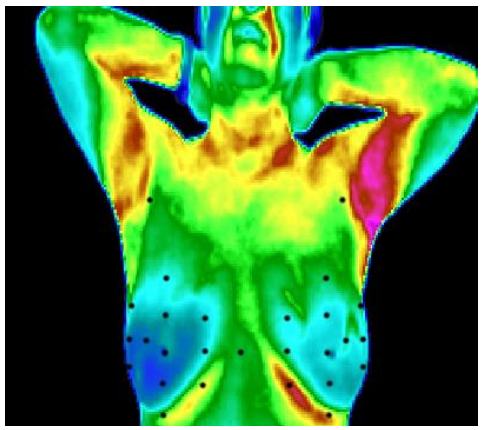

Figure 8. Acupoint positioning results of the infrared thermogram of the front chest

5. EXPERIMENTS AND RESULTS ANALYSIS

To verify the effectiveness of our automatic acupoint positioning algorithm, this paper sets up a preliminary data library for the chest infrared thermograms of breast cancer patients after surgery. The images were shot at the temperature of 23±1℃, and the humidity of 60%±5%. The shooting environment is slightly dark, with no wind, dust, or strong thermal radiation sources. During the shooting, the patient was asked to sit quietly in the shooting environment for 30min to adapt to the room temperature, and calm down their feelings. After that, he/she sat 1.5m before an infrared camera, and held breath for several seconds. Then, the thermal imager took infrared images of the front chest and upper limbs. During the experiment, 130 front infrared thermograms of different patients were selected from the image library to test the effect of chest acupoint positioning.

The temperature specific algorithm and edge extraction algorithm are both associated with temperature distribution. According to the different body temperature features of the subjects, the temperature distribution interval (the difference between highest and lowest temperatures) of the infrared thermograms was divided into three classes: normal temperature difference, small temperature difference, and large temperature difference. Table 2 shows the number and proportion of each class.

The reliability of the automatic acupoint positioning algorithm of infrared thermograms was evaluated by accuracy, i.e., the probability of correctly positioning an organ/acupoint in several chest infrared thermograms. The higher the accuracy, the better the positioning effect. The inverse is also true. During chest organ positioning, the organs related to acupoint positioning were selected: In the horizontal direction, supraclavicular fossae, armpits, and nipples were selected; In the vertical direction, left armpit, left nipple, left supraclavicular fossa, anterior median line, right supraclavicular fossa, right nipple, and right armpit were chosen. The test results are reported in Tables 3 and 4.

Table 2. Infrared thermograms in different temperature distribution intervals

Class	Range	Number	Proportion
Normal	3-5°C	91	70%
Large	4-8°C	14	10.77%
Small	0-2°C	25	19.23%

Table 3. Horizontal positioning accuracies

Positioning part	Normal temperature difference	Large temperature difference	Small temperature difference
Supraclavicular fossae	100.00%	93.33%	94.62%
Armpits	97.65%	98.92%	97.92%
Nipples	91.30%	92.33%	89.31%

Table 4. Vertical positioning accuracies

Positioning part	Normal temperature difference	Large temperature difference	Small temperature difference
Left armpit	97.83%	83.33%	92.31%
Left nipple	97.65%	98.92%	97.92%
Left supraclavicular fossa	92.30%	85.33%	90.31%
Anterior median line	100.00%	100.00%	98.23%
Right supraclavicular fossa	98.46%	86.73%	94.56%
Right nipple	96.45%	97.82%	95.12%
Right armpit	93.30%	86.33%	92.45%

Table 5. Positioning accuracies of front chest acupoints

Acupoint	Accuracy	Acupoint	Accuracy
Bulang	95.52%	Shenfeng	93.12%
Lingxu	90.24%	Wuyi	95.52%
Yingchuang	90.12%	Ruzhong	96.56%
Rugen	92.02%	Shidou	91.12%
Tianxi	93.24%	Xiongxiang	90.78%
Qimen	96.79%	Zhongfu	94.72%
Tianchi	90.88%		

Since the temperature in a small area near a chest acupoint would change simultaneously, it is not necessary to fix the acupoint at a specific point during the positioning. That is, a small deviation is tolerable. This is known as the tolerance of the positioning algorithm. Through observation, it is learned that an acupoint can be considered correctly located, if the position falls within the circle centering on the exact acupoint position, with a radius of 3 pixels. Hence, the positioning accuracies of front chest acupoints were obtained (Table 5).

6. CONCLUSIONS

This paper presents an automatic positioning algorithm for chest acupoints based on infrared thermograms. Firstly, the chest organs were located in the original infrared thermogram. Then, the chest acupoints were positioned automatically, according to the relative position between chest organs and each acupoint. In our algorithm, the acupoints are positioned essentially from coarse positioning to fine positioning, based

on the fusion of multiple features. The coarse positioning determines the rough areas of chest organs, in view of their spatial distribution. The fine positioning determines the specific coordinates of the organs, using the temperature specificity and temperature edges in the organ area. This positioning approach prevents the disturbance of similar temperature distributions of different organs, and improves the positioning accuracy. In addition, the computing is confined in an independent area to simplify the feature analysis, thereby reducing the computing complexity. As a result, our approach operates faster and resists disturbance better than the traditional positioning algorithms solely based on temperature variation.

ACKNOWLEDGEMENT

This research was supported by Zhejiang Provincial Basic Public Welfare Research Project (Grant No.: LGF20H290002).

REFERENCES

[1] Tachibana, K., Ueki, N., Uchida, T., Koga, H. (2012). Randomized comparison of the therapeutic effect of acupuncture, massage, and Tachibana-style-method on stiff shoulders by measuring muscle firmness, VAS, pulse, and blood pressure. Evidence-Based Complementary and Alternative Medicine, 2012: 989705. https://doi.org/10.1155/2012/989705

[2] Takayama, S., Kamiya, T., Watanabe, M., Hirano, A., Matsuda, A., Monma, Y., Yaegashi, N. (2012). Report on disaster medical operations with acupuncture/massage therapy after the great East Japan earthquake. Integrative Medicine Insights, 7(7): 1-5. https://doi.org/10.4137/IMI.S9541

[3] Klassen, E., Wiebelitz, K.R., Beer, A.M. (2019). Classical massage and acupuncture in chronic back pain–non-inferiority randomised trial. Zeitschrift für Orthopädie und Unfallchirurgie, 157(3): 263-269. https://doi.org/10.1055/a-0715-2332

[4] Liu, H.Y. (2013). Study on the prevention of lymphedema of the upper limb on the affected side after breast cancer surgery by moxibustion and acupoint combined massage. Northern Pharmacy, 10(5): 73-74. https://doi.org/CNKI:SUN:BFYX.0.2013-05-066

[5] Wan, H. (2019). Observation of therapeutic effect of acupoint massage on upper limb lymphedema after breast cancer operation. Chinese Community Physician, 35(20): 100-101. https://doi.org/10.3969/j.issn.1007-614x.2019.20.071

[6] Fink, J., Burns, J., Perez Moreno, A.C., Kram, J.J., Armstrong, M., Chopp, S., Conway, N. (2020). A quality brief of an oncological multisite massage and acupuncture therapy program to improve cancer-related outcomes. The Journal of Alternative and Complementary Medicine, 26(9): 822-826. https://doi.org/10.1089/acm.2019.0371

[7] Ijaz, N., Welsh, S., Boon, H. (2020). A survey of acupuncture-providing registered massage therapists in Ontario, Canada: motivation, training, and practice characteristics. International Journal of Therapeutic Massage & Bodywork, 13(3): 18-29. https://doi.org/10.3822/ijtmb.v13i3.505

[8] Elahee, S. F., Mao, H. J., Zhao, L., Shen, X. Y. (2020). Meridian system and mechanism of acupuncture action: A scientific evaluation. World Journal of Acupuncture-Moxibustion, 30(2): 130-137. https://doi.org/10.1016/j.wjam.2020.05.003

[9] Chang, Y., Tieming, M. (2019). Application of infrared thermal imaging technology in the study of human acupoint specificity. Journal of Liaoning University of Traditional Chinese Medicine, 2019.

[10] Huang, J.H., Xia, Q.G., Feng, X.X., Ge, L.B., Shen, X.Y., Hu, S.F., Ying, J. (2012). Study on Surface Infrared Radiation Spectrum of Guanyuan (RN4) between Breast Cancer Patients after Mastectomy and Patients with Hyperplasia of Mammary Glands. Chinese Archives of Traditional Chinese Medicine, 30(9): 3. https://doi.org/CNKI:SUN:ZYHS.0.2012-09-012

[11] Shen, X., Ding, G., Zhu, J., Yao, W., Huang, Z., Yang, W., Fei, L. (2001). Human acupoints and moxibustion infrared radiation spectrum with infrared transmission in acupoints. Acta University Tradition Medicinal Science Pharmacologiaeque Shanghai, 15(4): 33-35.

[12] Park, K., Chae, M., Cho, J. H. (2021). Image pre-processing method of machine learning for edge detection with image signal processor enhancement. Micromachines, 12(1): 73. https://doi.org/10.3390/mi12010073

[13] Gonçalves, C.B., de Souza, J.R., Fernandes, H. (2022). CNN architecture optimization using bio-inspired algorithms for breast cancer detection in infrared images. Computers in Biology and Medicine, 142: 105205. https://doi.org/10.1016/j.compbiomed.2021.105205

[14] Ryu, J.B., Park, H.H., Park, J. (2011). Corner classification using Harris algorithm. Electronics Letters, 47(9): 536-538. https://doi.org/10.1049/el.2011.0594

[15] Wang, F., Zhang, B., Zhang, C., Zhang, C., Wang, M. (2021). A multispectral image enhancement algorithm based on frame accumulation and LOG detection operator. In Artificial Intelligence in China, 334-343. https://doi.org/10.1007/978-981-15-8599-9_39

[16] Wu, Z.C. (2014). Large Atlas of Human Meridian and Acupoint Standards. China Light Industry Pres.

[17] Zhang, J. (2017). National Institutes of Health, Standard Health Questionnaire and Anthropometric Methods. RTI Institute, Shanghai Science and Technology Press, 2017

[18] Deng, L.Y. (2002). Liangyue, Wall Chart of National Standard Meridian Points (Female). China Traditional Chinese Medicine Press.